Available online at www.sciencedirect.com
SCIENCE DIRECT®
Journal of Nuclear Materials 340 (2005) 307–314
journal of nuclear materials
www.elsevier.com/locate/jnucmat

Mechanism of dynamic strain aging and characterization of its effect on the low-cycle fatigue behavior in type 316L stainless steel

Seong-Gu Hong, Soon-Bok Lee *

Department of Mechanical Engineering, Korea Advanced Institute of Science and Technology, 373-1 Guseong-dong, Yuseong-gu, Daejeon 305-701, Republic of Korea

Received 21 October 2004; accepted 22 December 2004

Abstract

Low-cycle fatigue tests were carried out in air in a wide temperature range from 20 to 650 °C with strain rates of 3.2×10^{-5}–1×10^{-2} s^{-1} for type 316L stainless steel to investigate dynamic strain aging (DSA) effect on the fatigue resistance. The regime of DSA was evaluated using the anomalies associated with DSA and was in the temperature range of 250–550 °C at a strain rate of 1×10^{-4} s^{-1}, in 250–600 °C at 1×10^{-3} s^{-1}, and in 250–650 °C at 1×10^{-2} s^{-1}. The activation energies for each type of serration were about 0.57–0.74 times those for lattice diffusion indicating that a mechanism other than lattice diffusion is involved. It seems to be reasonable to infer that DSA is caused by the pipe diffusion of solute atoms through the dislocation core. Dynamic strain aging reduced the crack initiation and propagation life by way of multiple crack initiation, which comes from the DSA-induced inhomogeneity of deformation, and rapid crack propagation due to the DSA-induced hardening, respectively.

1. Introduction

The reactor vessels and piping systems in liquid metal cooled fast breeder reactor (LMFBR) are exposed to severe conditions, such as high temperature ranging from 300 to 600 °C, and undergo temperature-gradient induced cyclic thermal stresses as a result of start-ups and shut-downs. In these applications, low-cycle fatigue (LCF) represents a predominant failure mode and, thus, specific attention on LCF is needed in the design and life assessment of such components. Type 316L stainless steel is a prospective material for LMFBR applications because of a good combination of its excellent high-temperature tensile and creep strength, corrosion resistance, and enhanced resistance to sensitization and associated intergranular cracking. It has been reported that, in the temperature range of 300–600 °C where LMFBR operates, type 316L stainless steel is susceptible to dynamic strain aging (DSA) which may induce a significant change in material properties such as strength and ductility [1–4]. Therefore, to apply type 316L stainless steel to LMFBR applications, more detailed research for the influence of DSA on LCF behavior is required in this temperature region.

* Corresponding author. Tel.: +82 42 869 3029; fax: +82 42 869 3210.
E-mail address: sblee@kaist.ac.kr (S.-B. Lee).

0022-3115/$ - see front matter © 2005 Elsevier B.V. All rights reserved.
doi:10.1016/j.jnucmat.2004.12.012

In this study, the effect of DSA on LCF behavior was investigated by performing low-cycle fatigue tests. The condition for DSA to occur was evaluated using the anomalies associated with DSA and the mechanism of DSA was studied by calculating the activation energies for the onset of each type of serrated yielding. The reduction of fatigue resistance with an increase in temperature and a decrease in strain rate was investigated in the viewpoint of the influence of DSA on crack initiation and propagation.

2. Experiment

2.1. Material and specimen

The material used in this study was cold-worked (CW) 316L stainless steel having the following chemical composition in wt%: C–0.025, Si–0.41, Mn–1.41, P–0.025, S–0.025, Ni–10.22, Cr–16.16, Mo–2.09, N–0.043, Fe–balance. The as-received material was manufactured by the following processes: the material was solution-treated at 1100 °C for 40 min, then water-quenched, and, finally, a round bar with a diameter of 16 mm was made through the cold-drawing, which introduced a tensile pre-strain of 17%. This treatment yielded an average intercept grain size of 44.2 μm. The as-received material was fabricated into dog-bone type specimens with a gauge length of 36 mm and a gauge diameter of 8 mm in accordance with ASTM standard E606-92.

2.2. Test equipment and procedure

A closed-loop servo-hydraulic test system with 5-ton capacity was used to perform LCF tests, and a 3-zone resistance type furnace which can control temperature within a variation of ±1 °C at steady state was used for temperature control. A high temperature extensometer (MTS model no.: 632-13F-20) was used to measure strain and control strain signal.

LCF tests were carried out in air under a fully reversed total axial strain control mode with a triangular waveform at room temperature (RT), 200, 400, 550, 600, and 650 °C. A strain amplitude was fixed at 0.5% and strain rates varied from 3.2×10^{-5} to 1×10^{-2} s^{-1}.

The fracture surfaces of LCF failed specimens were examined by SX-30E scanning electron microscope (SEM) to investigate the mechanism of crack initiation and propagation. The mechanism of plastic deformation was studied by JEOL 2000FX transmission electron microscope (TEM). Samples for TEM were obtained from thin slice cut at a distance of 1mm away from the fracture surface and then electropolished in a solution containing 5% perchloric acid and 95% acetic acid at 70 V and 10 °C.

3. Results and discussion

3.1. The regime of DSA

Dynamic strain aging is the phenomenon of interaction between diffusing solute atoms and mobile dislocations during plastic deformation and depends on deformation rate and temperature, which govern the velocities of mobile dislocations and diffusing solute atoms, respectively. The occurrence of DSA can be manifested by the anomalous features of material behavior, which are induced by DSA. While serrated yielding is the most commonly observed manifestation of DSA, there are various other concurrent phenomena. Other anomalies associated with DSA have been described by Rodriguez [5]: during monotonic tensile deformation, DSA is manifested by the serrated flow in the stress–strain curve, the peak or the plateau in the variation of material strength with temperature, the minima in the variation of ductility with temperature, and the negative strain-rate sensitivity (SRS). Hong and Lee [4] reported that, however, the anomalies related to DSA during LCF deformation are somewhat different from those in tensile loading. Dynamic strain aging under LCF loading in type 316L stainless steel, the same material in the present study, is manifested in the forms of the negative temperature dependence of cyclic peak stress, the negative temperature dependence of plastic strain amplitude or softening ratio (an amount of cyclic softening until half-life), the negative SRS, and the negative strain rate dependence of plastic strain amplitude or softening ratio. It is noted that serrated yielding is not observed in the stress–strain hysteresis loops. This absence is thought to result from the total strain amplitude of 0.5% used in LCF tests being too small compared with the critical strain that is needed for serrated yielding to occur: during tensile deformation, serrated yielding appears at strains above 1% [4]. This fact implies that DSA commences earlier than is manifested in the form of serrated yielding, and, thus, determining the regime of DSA should be done with caution.

Based on the anomalies associated with DSA [4], the regime of DSA under LCF loading was in the temperature range of 250–550 °C at a strain rate of 1×10^{-4} s^{-1}, in 250–600 °C at 1×10^{-3} s^{-1}, and in 250–650 °C at 1×10^{-2} s^{-1}.

3.2. The mechanism of DSA

The mechanism of DSA can be identified by evaluating the activation energy values for DSA and comparing them with those values reported in the literature because DSA is the thermally activated process associated with interaction between diffusing solute atoms and mobile dislocations. There are several methods to evaluate the activation energy for DSA, and most of them are related

to the serrated yielding phenomena. As mentioned in Section 3.1, unfortunately, serrated yielding didn't appear in the stress–strain hysteresis loops during LCF deformation. It is noticed that, however, the regime of DSA under LCF loading is consistent with that in tensile loading [4]. Hence, it is thought to be reasonable to use the results of tensile tests in order to evaluate the activation energy for DSA under LCF loading. The methods for evaluating the activation energy associated with serrated yielding can be described as follows: (1) activation energy, Q, can be obtained from the relationship between the critical strain, temperature and strain rate for the onset of serrated yielding [6–8]. (2) Q can be obtained from the relationship between temperature and strain rate for the onset of serrated yielding [9]. (3) Q can be obtained from the measurement of stress drop as suggested by Pink and Grinberg [10]. It has been reported that the calculated activation energy values using the different methods are close agreement with each other [11,12]. There is no significant difference. Hence, the second method was adopted in the present study. Cottrell [9] suggested the DSA model for the onset of serrated yielding assuming that solute atmospheres are dragged by dislocations moving at less than a critical velocity. This model gives the relationship between temperature and strain rate for the onset of serrated yielding, as like Eq. (1):

$$\dot{\varepsilon} = \frac{4b\rho C_v D_0}{l} \exp\left(\frac{-Q}{kT}\right), \tag{1}$$

where b, ρ, C_v, D_0, l, Q, and k represent the Burgers vector, the dislocation density, the vacancy concentration, the diffusion frequency factor, the effective radius of the atmosphere, the activation energy for solute migration, and the Boltzmann constant, respectively.

Typical segments of the stress–strain curves from tensile tests are shown in Fig. 1. The different types of serrations, which follows the generally accepted nomenclature in Ref. [5], appeared in the stress–strain curves with temperature. At a given strain rate, type D serration was observed at low temperatures, type A + B + E serrations at intermediate temperatures, and type A + B + C + E serrations at high temperatures. The condition for the occurrence of serrated yielding is presented in Fig. 2. Following Eq. (1), the activation energy for the onset of serrated yielding can be obtained from the slope of the boundaries delineating different serrated flow regimes in a $\ln\dot{\varepsilon} - 1/T$ plot (Fig. 2). The calculated values of activation energy for each type of serration are indicated in Fig. 2. They were 75.3 kJ/mol for type D serration (Q_D), 182.2 kJ/mol for type A + B + E serrations (Q_{ABE}), and 205.3 kJ/mol for type A + B + C + E serrations (Q_{ABCE}). Three different activation energy values in the temperature range of serrated flow indicate that serrated yielding in CW 316L stainless steel is attributed to more than one mechanism.

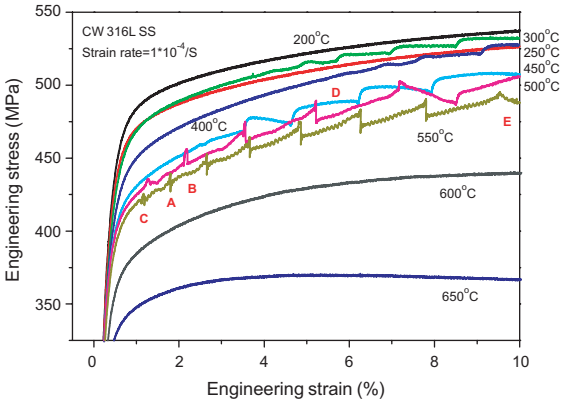

Fig. 1. Segments of the stress–strain curves from tensile tests.

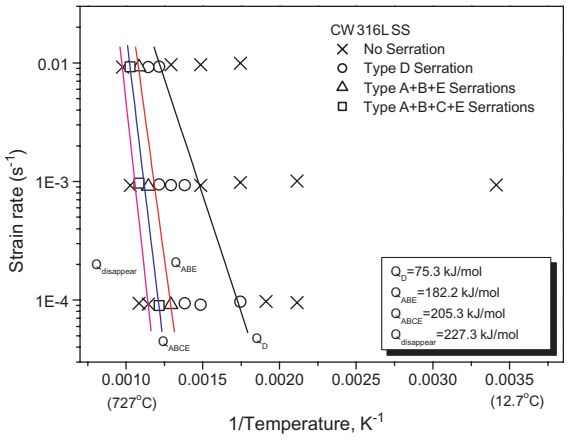

Fig. 2. Regimes of occurrence of serrated yielding under tensile loading.

In austenitic stainless steel, DSA occurs in a wide range of temperature from 200 to 800 °C [13,14]. According to Jenkins and Smith [15], at low temperatures below 450 °C, interstitial atoms (C or N) are responsible for serrated yielding, whereas, at high temperatures, the diffusion of chromium atoms causes serrated flow. Q values for bulk diffusion of interstitial and substitutional solutes in γ-Fe are about 134 and 400 kJ/mol, respectively. Considering the activation energies for diffusion of carbon and nitrogen in γ-Fe, their values are similar and, thus, their influence on DSA is considered to be equivalent. Samuel et al. [12] have reported Q values, obtained from the second method (Eq. (1)), in type 316 stainless steel. Q values are 133 kJ/mol at low temperatures (250–350 °C) and 278 kJ/mol at high temperatures (400–650 °C). Diffusions of interstitial solutes and substitutional solutes like Cr to dislocations are considered as the mechanisms responsible for serrated flow in the low and high temperature

regimes, respectively. The similar result has been reported in type 316 stainless steel [16].

It is noticed that Q values from the literature are much larger than the observed values in the present study. The lower observed values of activation energy for DSA have been attributed to strain-induced diffusion [17] or pipe diffusion [18] along the dislocation core. Cuddy and Lesile [18] have suggested that substitutional solutes can diffuse rapidly along the dislocation core with the activation energy which may be 0.4–0.7 times the activation energy for bulk diffusion in α-Fe. The required features for the mechanism of DSA through pipe diffusion are provided by the dislocation arrest model [19], originally proposed by Sleeswyk [6]. This model suggests that solute atmospheres form on forest dislocations and, then, drain by pipe diffusion from forest dislocations to mobile dislocations while mobile dislocations are temporarily arrested at forest dislocations to overcome them through thermal activation process (Fig. 3). Since this model does not require bulk diffusion through crystal lattice to form solute atmospheres on mobile dislocations, the lower activation energy, compared with that of bulk diffusion, can be achieved. The pipe diffusion through the dislocation core will be rapid enough to allow the formation of solute atmospheres on the mobile dislocations without requiring any enhancement since solute atmospheres need not pin the entire dislocation line to have an effect, but merely the portion of the dislocation line, intersecting with the forest dislocations.

The calculated values of activation energy in the present study were about 0.57–0.74 times the activation energies for lattice diffusion: $Q_{\mathrm{D}} \approx 0.57 \cdot Q^{\mathrm{bulk}}_{\mathrm{CorN}}$, $Q_{\mathrm{ABE}} \approx 0.66 \cdot Q^{\mathrm{bulk}}_{\mathrm{Cr}}$, and $Q_{\mathrm{ABCE}} \approx 0.74 \cdot Q^{\mathrm{bulk}}_{\mathrm{Cr}}$. For f.c.c. crystals, the forest dislocations, which intersect the slip planes, are the essential barriers to the motion of the dislocations lying on the slip planes [20]. Moreover, the material used in this study has originally involved high density of forest dislocations because it was made through the cold-drawing (refer to Fig. 6(a) in Ref. [4]). Therefore, it is thought to be reasonable to infer that serrated yielding in CW 316L stainless steel is caused by the pipe diffusion of solute atoms through the dislocation core: type D serration results from the pipe diffusion of interstitial solutes, such as C or N, and the pipe diffusion of substitutional Cr is responsible for type A + B + E or A + B + C + E serrations.

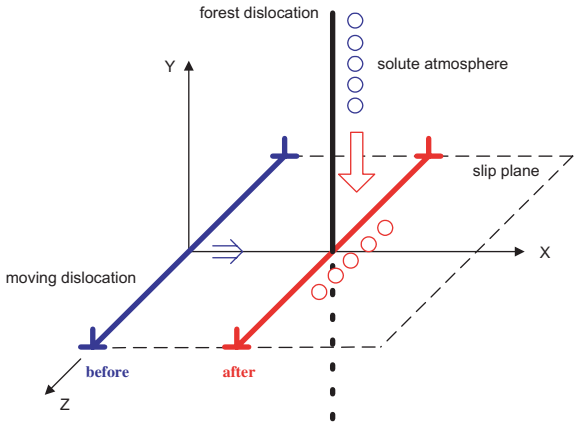

Fig. 3. Schematic drawing depicting the mechanism of DSA through pipe diffusion.

3.3. Microstructures

As shown in Fig. 4, the dislocation structure changed from a (elongated) cellular structure at temperatures below 250 °C to a planar structure in the temperature range of 250–600 °C (DSA regime), and back to a (equi-axial) cell at high strain rates or a subgrain structure at low strain rates beyond 600 °C. This fact indicates that the mechanism of plastic deformation changes from wavy slip mode in the non-DSA regime to planar slip mode in the regime of DSA.

DSA-induced hardening, manifested by the anomalies associated with DSA in Section 3.1, is thought to come from the following two mechanisms: (1) based on the impurity pinning model [21], DSA is a consequence of the pinning and regeneration of dislocations. The pinning of dislocations during deformation could result from the formation of either Snoek or Cottrell atmospheres. As the dislocations are immobilized by pinning, more dislocations have to be generated to maintain the imposed strain rate. The enhancement in dislocation density as a result of such a process has been revealed by TEM studies [2,22]. (2) As shown in Fig. 4(b) and (c), in the regime of DSA, the mechanism of interaction between mobile dislocations and solute atmospheres enhances the slip planarity and, thus, restricts the cross slip of screw dislocations. This results in the reduction of dynamic recovery.

It is noted that slip planarity is enhanced (that is, DSA effect becomes more pronounced) with a decrease in strain rate, as shown in Fig. 4(b) and (c). This is attributed to the extension of the temporary arrest time of moving dislocations at forest dislocations, t_{w}, which is inversely related to strain rate, with a decrease in strain rate.

3.4. DSA effect on the fatigue resistance

The variation of fatigue life, defined as a 30% load drop point of a peak stress at half-life, with temperature and strain rate is presented in Fig. 5. At a given strain rate, a drastic reduction of fatigue life was observed with an increase in temperature, and this tendency became more pronounced with an increase in strain rate (Fig. 5(a)). As shown in Fig. 5(b), fatigue life reduced with

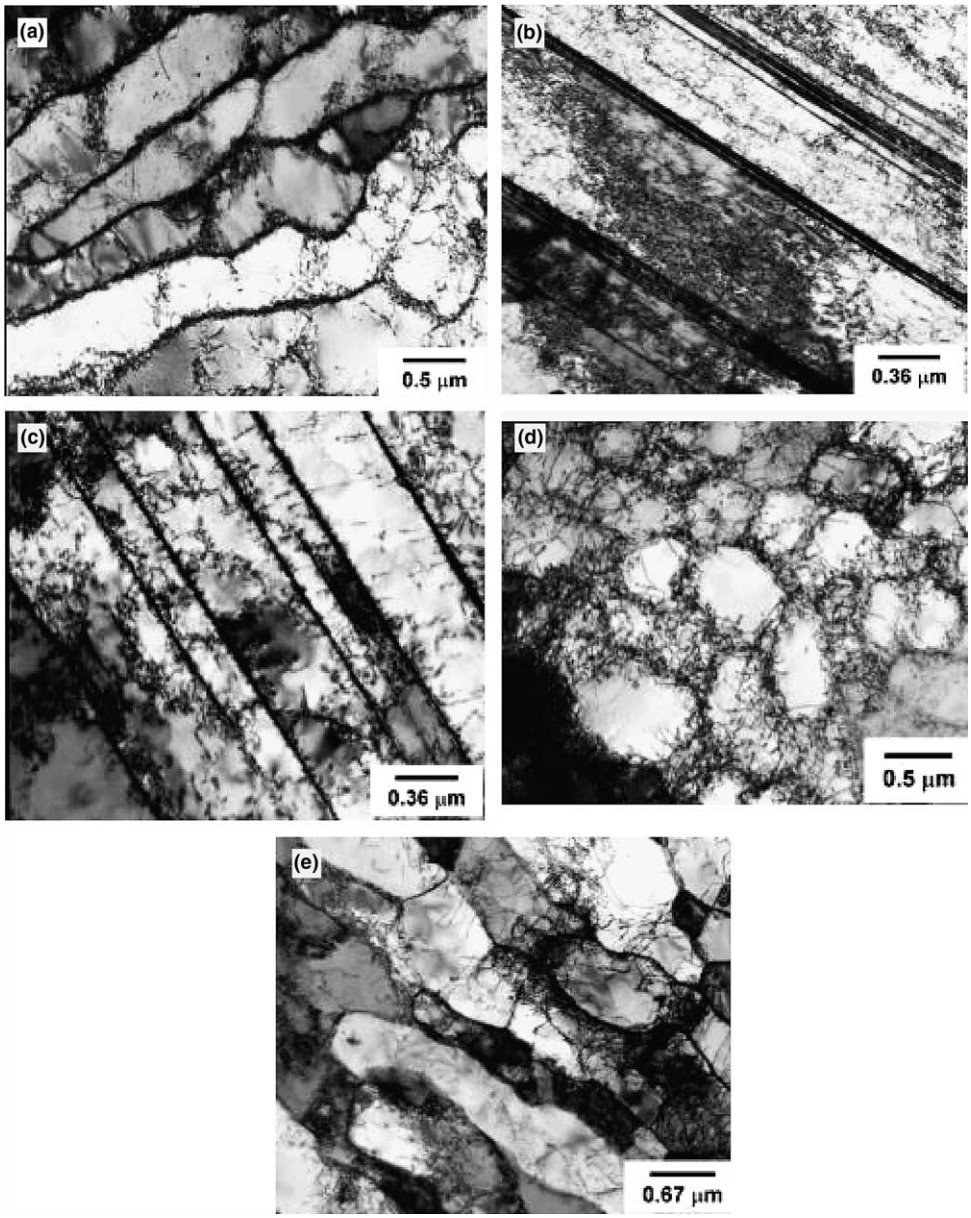

Fig. 4. TEM micrographs depicting the substructures at $\Delta\varepsilon_t/2 = 0.5\%$: (a) RT, $\dot{\varepsilon} = 1 \times 10^{-3}$ s^{-1}, (b) 400 °C, $\dot{\varepsilon} = 1 \times 10^{-2}$ s^{-1}, (c) 400 °C, $\dot{\varepsilon} = 1 \times 10^{-4}$ s^{-1} [4], (d) 650 °C, $\dot{\varepsilon} = 1 \times 10^{-2}$ s^{-1}, and (e) 650 °C, $\dot{\varepsilon} = 3.2 \times 10^{-5}$ s^{-1} [4].

a decrease in strain rate at a given temperature, and the strain rate dependence of fatigue life was accelerated as temperature decreased in the temperature range of 400–650 °C.

In austenitic stainless steels [1–3], a reduction of fatigue resistance has been reported at elevated temperature, and it is attributed to creep, oxidation, and DSA effects or interaction among these factors. However, it should be noted that the effects of creep and oxidation become more pronounced as temperature increases or strain rate decreases. This will produce the opposite prediction, compared with the present results. Hence, creep and oxidation effects were not enough to account for the variation of the fatigue resistance with temperature and strain rate, observed in the present study. This fact could be also confirmed by observing the fracture surfaces of LCF failed specimens with SEM. In the regime of DSA, there were no remarkable evidences of creep or oxidation (Fig. 6(c) and (d)): fatigue cracks initiated at the slip bands connected to the surface. Initial

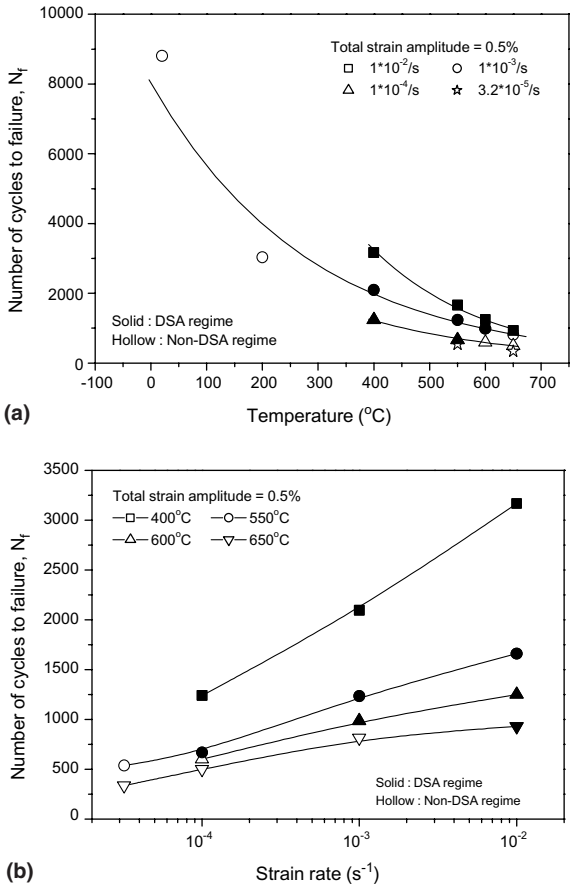

Fig. 5. The variation of fatigue life with (a) temperature and (b) strain rate.

propagation occurred along slip planes oriented at 45° to the applied stress axis designated as stage I. The initial propagation was confined to the active slip planes as evidenced by the cleavage facets in Fig. 6(c). This type of cracking continued through only a few grains before the transition to stage II transgranular cracking, evidenced by striations on the fracture surface, occurred. That is, there was no evidence of intergranular cracking or damage which can be induced by creep. Oxidation became important only at high temperatures above 600 °C with low strain rates below $1 \times 10^{-4}\ s^{-1}$ where DSA disappeared. Therefore, the temperature and strain rate dependence of fatigue resistance could be explained by the DSA effect.

When dynamic strain aging operates, the planar dislocation structure is developed, as shown in Fig. 4(b) and (c), and, thus, plastic deformation is localized on the slip bands. This localized deformation on slip bands, if connected to the surface, could be served as crack initiation sites, which were evidenced by the cleavage facets shown in Fig. 6(c) and (d), and resulted in the multiplication of crack initiation site. This mechanism reduced the crack initiation life. Similar results have been reported in other materials. In alloy 800H [23], the effects of DSA on crack initiation life and evolution of the microcrack density with the number of cycles have been studied and compared with the result in vacuum, to exclude the effect of environment on crack initiation. The results reveal that DSA leads to an appreciably higher crack density and an overall decrease in crack initiation life. In the study on SA508 [24], dynamic strain aging increases the degree of inhomogeniety of deformation during LCF deformation by solute locking of moving dislocations so that DSA enhanced the partitioning of cyclic strains into separate regions. This localized deformation leads to multiple crack initiation.

The crack propagation rate can be described by Eq. (2) [25,26]:

$$\frac{dl}{dN} \propto (\Delta\sigma)^{\alpha} \cdot l^{\beta}, \tag{2}$$

where l, α, and β are the crack length and material constants, respectively. For a given strain amplitude, the crack propagation rate will increase with an increase in the developed stress. As mentioned in Section 3.3, the mechanism of DSA introduces the hardening of the material, characterized by the negative temperature dependence of flow stress and the negative strain rate sensitivity. This results in the development of a higher stress with an increase in temperature or a decrease in strain rate, at a given strain. Therefore, a higher stress concentration at the crack tip, in the regime of DSA, will enhance the crack propagation rate and lead to the reduction in crack propagation life. It is also noted that, at a given temperature where DSA operates, the reduction in crack propagation life increases with a decrease in strain rate because of the negative strain rate sensitivity. This is consistent with the present results shown in Fig. 5. Abdel-Raouf et al. [27] examined the elevated temperature fatigue deformation characterization of Ferrovac E iron and reported that DSA causes a reduction in crack propagation life: crack tips grow continuously until their blunting occurs by sufficient dislocations motion, operating in a cross-slipping manner to accommodate curvature of the crack front. However, prevention of plasticity, in the regime of DSA, by continuous locking of dislocations reduces the degree of blunting causing the crack to propagate more rapidly. The crack propagation tests of type 316L(N) stainless steel [28] also revealed the consistent result. The crack propagation rate is significantly increased in the regime of DSA, compared with that in the non-DSA regime, because DSA-induced embrittlement restricts plasticity at the crack tip and, thus, retards blunting of the propagating crack, resulting in a higher crack propagation rate.

Based on the results, it was found that DSA reduced both crack initiation and propagation life, resulting in

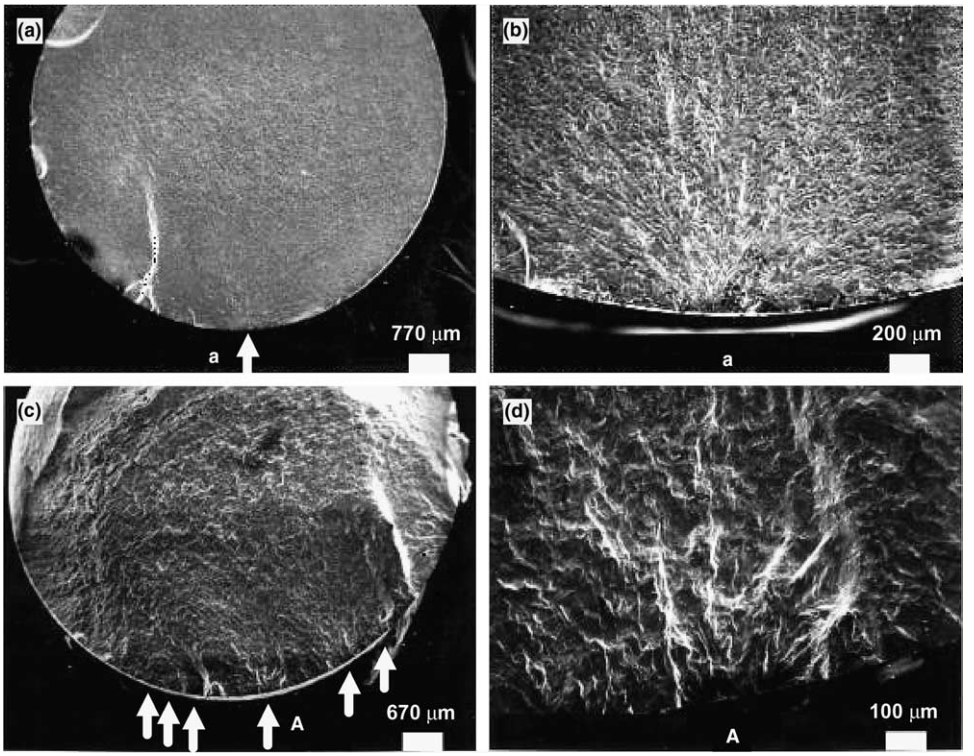

Fig. 6. SEM micrographs showing the fracture surfaces at $\Delta\varepsilon_t/2 = 0.5\%$: (a, b) RT, $\dot{\varepsilon} = 1 \times 10^{-3}$ s^{-1}, (c, d) 550 °C, $\dot{\varepsilon} = 1 \times 10^{-2}$ s^{-1} [3].

the reduction of fatigue resistance. Considering that the temperature for DSA to operate moves to a higher temperature with an increase in strain rate and, in the regime of DSA, the DSA effect becomes more pronounced with a decrease in strain rate; the variation of fatigue life with temperature and strain rate shown in Fig. 5 can be explained.

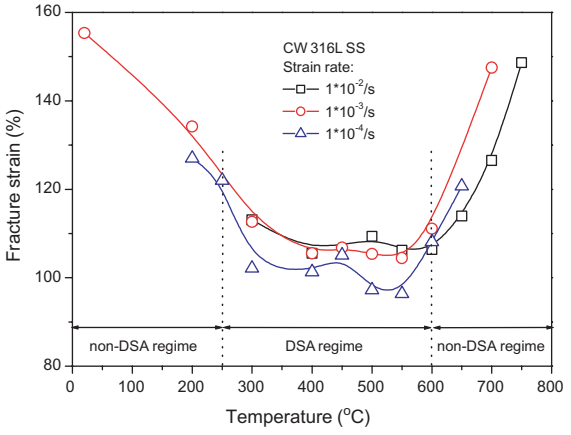

Fig. 7. The variation of material ductility with temperature and strain rate.

The reduction of fatigue resistance in the regime of DSA can be also accounted for in the viewpoint of the change in material ductility. According to Landgraf [29], low-cycle fatigue life is dominated by material ductility. Since DSA induces the embrittlement of the material, causing the reduction in material ductility (Fig. 7), fatigue resistance will decrease in the regime of DSA.

4. Conclusions

(1) Dynamic strain aging occurred within a certain range of temperature and strain rate during LCF deformation. The regime of DSA was in the temperature range of 250–550 °C at a strain rate of 1×10^{-4} s^{-1}, in 250–600 °C at 1×10^{-3} s^{-1}, and in 250–650 °C at 1×10^{-2} s^{-1}.

(2) The mechanism of DSA changed with temperature and strain rate. It seems to be that, at low temperatures where type D serration appears, DSA occurs by pinning of dislocations through the pipe diffusion of the interstitial atoms such as *C* or *N* along the dislocation core, and, at high temperatures where type A + B + E or type A + B + C + E serrations appear, the pipe diffusion of substitutional Cr along the dislocation core is responsible for DSA.

(3) The mechanism of plastic deformation changed from wavy slip mode in the non-DSA regime to planar slip mode in the regime of DSA because, in the regime of DSA, the mechanism of interaction between mobile dislocations and solute atmospheres enhances the slip planarity.

(4) A steep reduction of fatigue resistance was observed in the regime of DSA. Dynamic strain aging reduced the crack initiation and propagation life by way of multiple crack initiation, which comes from the DSA-induced inhomogeneity of deformation, and rapid crack propagation due to the DSA-induced hardening, respectively.

Acknowledgement

This work was supported by Computer Aided Reliability Evaluation (CARE) National Research Laboratory in Korea Advanced Institute of Science and Technology (KAIST).

References

[1] V.S. Srinivasan, R. Sandhya, K. Bhanu Sankara Rao, S.L. Mannan, K.S. Raghavan, Int. J. Fatigue 13 (6) (1991) 471.
[2] V.S. Srinivasan, M. Valsan, R. Sandhya, K. Bhanu Sankara Rao, S.L. Mannan, D.H. Sastry, Int. J. Fatigue 21 (1999) 11.
[3] S.G. Hong, S.B. Lee, Int. J. Fatigue 26 (8) (2004) 889.
[4] S.G. Hong, S.B. Lee, J. Nucl. Mater. 328 (2–3) (2004) 232.
[5] P. Rodriguez, in: Encyclopedia of Materials Science and Engineering, Suppl. vol. 1, Pergamon, New York, 1988, p. 504.
[6] A.W. Sleeswyk, Acta Metall. 6 (1958) 598.
[7] A. van den Beukel, Acta Metall. 28 (1980) 965.
[8] P.G. McCormick, Acta Metall. 20 (1972) 351.
[9] A.H. Cottrell, in: Dislocations and Plastic Flow in Crystals, Oxford University, London, 1953.
[10] E. Pink, A. Grinberg, Acta Metall. 30 (1982) 2153.
[11] S. Venkadesan, C. Phaniraj, P.V. Sivaprasad, P. Rodriguez, Acta Metall. Mater. 40 (3) (1992) 569.
[12] K.G. Samuel, S.L. Mannan, P. Rodriguez, Acta Metall. 36 (8) (1988) 2323.
[13] L.H. de Almeida, S.N. Monteiro, in: Proceedings of the Second International Conference on Mechanical Behavior of Materials, Boston, 1976, p. 1697.
[14] C. Gupta, J.K. Chakravartty, S.L. Wadekar, J.S. Dubey, Mater. Sci. Eng. A 292 (2000) 49.
[15] C.F. Jenkins, G.V. Smith, Trans. Metall. Soc. AIME 245 (1969) 2149.
[16] S.L. Mannan, K.G. Samuel, P. Rodriguez, Trans. Ind. Inst. Metals 36 (1983) 313.
[17] R.W. Baluffi, Phys. Status Solidi 42 (1970) 11.
[18] L.J. Cuddy, W.C. Leslie, Acta Metall. 20 (1972) 1157.
[19] R.A. Mulford, U.F. Kocks, Acta Metall. 27 (1979) 1125.
[20] S. Nemat-Nasser, Y. Li, Acta Mater. 46 (2) (1998) 565.
[21] Y. Bergsrom, W. Roberts, Acta Metall. 19 (1971) 1243.
[22] A.S. Keh, Y. Nakada, W.C. Leslie, in: Dislocation Dynamics, McGraw-Hill, New York and London, 1968, p. 381.
[23] J. Bressers, in: Proceedings of the International Conference on High Temperature Alloys and Their Exploitable Potential, Elsevier Applied Science, Amsterdam, 1987, p. 385.
[24] M. Valsan, D.H. Sastry, K. Bhanu Sankara Rao, S.L. Mannan, Metall. Trans. A 25 (1995) 159.
[25] K. Yamaguchi, K. Kanazawa, S. Yoshida, Mater. Sci. Eng. 33 (1978) 175.
[26] B. Tomkins, Philos. Mag. 18 (1968) 1041.
[27] H. Abdel-Raouf, A. Plumtree, T.H. Topper, ASTM STP 519 (1973) 28.
[28] D.W. Kim, W.G. Kim, W.S. Ryu, Int. J. Fatigue 25 (2003) 1203.
[29] R.W. Landgraf, ASTM STP 467 (1970) 3.